Optimization-Based Distributed Flocking Control for Multiple Rigid Bodies

Tatsuya Ibuki, Sean Wilson, Junya Yamauchi, Masayuki Fujita, and Magnus Egerstedt

***Abstract*—This letter considers distributed flocking control on the Special Euclidean group for networked rigid bodies. The method captures the three flocking rules proposed by Reynolds: cohesion; alignment; and separation. The proposed controller is based only on relative pose (position and attitude) information with respect to neighboring rigid bodies so that it can be implemented in a fully distributed manner using only local sensors. The flocking algorithm is moreover based on pose synchronization methods for the cohesion/alignment rules and achieves safe separation distances through the application of control barrier functions. The control input for each rigid body is chosen by solving a distributed optimization problem with constraints for pose synchronization and collision avoidance. Here, the inherent conflict between cohesion and separation is explicitly handled by relaxing the position synchronization constraint. The effectiveness of the proposed flocking algorithm is demonstrated via simulation and hardware experiments.**

***Index Terms*—Multi-robot systems, optimization and optimal control, swarms.**

I. Introduction

FLOCKING, swarming, and schooling are common emergent collective motion behaviors exhibited in nature [1], [2]. These natural collective behaviors can be leveraged in multi-robot systems to safely transport large cohesive groups of robots within a workspace. To capture these effects, Reynolds introduced three heuristic rules: cohesion; alignment; and separation, to reproduce flocking motions in computer graphics in 1987 [3]. These rules have been applied by researchers in various fields including physics, biology, social science, and computer science [4]–[8]. The scope and flexibility of this motion coordination strategy have also caused it to be widely leveraged by robotics and control engineering communities to develop motion coordination control methods for multi-robot systems [9]–[19].

This letter tackles the 3-dimensional (3D) flocking control problem for multiple rigid bodies. The main goal is to develop a distributed control algorithm embodying the above three fundamental flocking rules while explicitly taking 3D attitude dynamics into account. Since these rules have an inherent conflict between cohesion and separation, this work aims to explicitly handle this conflict. Moreover, in order to enable application of the proposed algorithm in environments without global feedback, the information each rigid body needs to generate the flocking control inputs is reduced to relative information about neighboring rigid bodies. This information restriction enables each rigid body to implement a control law by using only local sensors, such as vision or infrared, without any other communication or global information. This feature, based only on local and relative information, is referred to as *fully distributed* in this letter.

Flocking control problems have been tackled by many researchers [10]–[19], where Reynolds's three rules are respectively considered as position synchronization (cohesion), attitude synchronization/velocity matching (alignment), and collision avoidance (separation). However, some flocking implementations regard an agent as a particle, i.e., its attitude is not considered [10]–[13]. Even in the case that attitudes are taken into consideration, to reduce complexity, 2D cases are often considered [14]–[17]. On the other hand, due to the conflict between cohesion and separation, related research often handles a subset of Reynolds's three rules, e.g., collision avoidance (separation) is not considered, or only alignment is achieved [13], [17], [18]. Compared with these studies, this work deals with rigid bodies with pose (position and attitude) dynamics on the *Special Euclidean group* $SE(3)$, and presents a distributed flocking algorithm to achieve all three rules simultaneously by solving a single optimization problem to minimize the conflict between cohesion and separation.

The research in [19] and [20] is the most related to this work. The authors in [19] also propose a 3D flocking algorithm incorporating the three rules. They provide theoretical guarantees on the achievement of alignment and separation behaviors. However, since their separation approach is based on an unbounded potential function, only the boundedness of the relative positions is proved for a cohesion behavior. Compared with that work, this letter newly proposes a flocking method with numerical optimization. This method guarantees a separation behavior and achieves a cohesion behavior as much as possible by minimizing a parameter to manage the conflict. The same optimization based approach is presented in [20] which can also achieve cohesion and separation behaviors. However, that work handles 2D ground vehicles and does not consider their attitudes, i.e., implicitly assumes the global attitude agreement among vehicles.

In summary, the main contribution of this letter is a novel 3D flocking algorithm based on distributed optimization to

Manuscript received September 10, 2019; accepted January 12, 2020. Date of publication January 28, 2020; date of current version February 11, 2020. This letter was recommended for publication by Associate Editor Prof. D. Lee and Editor Prof. N. Y. Chong upon evaluation of the reviewers' comments. This work was supported in part by JSPS KAKENHI under Grant 18K13775 and in part by the US National Science Foundation through Grant 1531195. *(Corresponding author: Tatsuya Ibuki.)*

T. Ibuki, J. Yamauchi, and M. Fujita are with the Department of Systems and Control Engineering, School of Engineering, Tokyo Institute of Technology, Tokyo 152-8550, Japan (e-mail: ibuki@sc.e.titech.ac.jp; yamauchi@sc.e.titech.ac.jp; fujita@ctrl.titech.ac.jp).

S. Wilson and M. Egerstedt are with the School of Electrical and Computer Engineering, Georgia Institute of Technology, Atlanta, GA 30332 USA (e-mail: Sean.T.Wilson@gatech.edu; magnus.egerstedt@ece.gatech.edu).

This letter has supplementary downloadable material available at http://ieeexplore.ieee.org, provided by the authors.

Digital Object Identifier 10.1109/LRA.2020.2969950

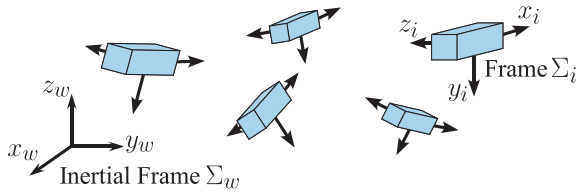

Fig. 1. Multiple rigid bodies in 3D space. Each rigid body has the rigid body motion as its motion dynamics. The available information for its control input is restricted to be relative information with respect to its neighbors.

minimize the conflict between cohesion and separation. We first define a rigid body network consisting of 3D pose dynamics and interconnection topology representing information flow between rigid bodies. Then, the control objective incorporating the three fundamental flocking rules is stated, and the optimization approach explicitly handling the conflict is explained. Here, cohesion, alignment, and separation are respectively considered as position synchronization, attitude synchronization, and collision avoidance. The proposed method is based on pose synchronization techniques [19] for cohesion/alignment and collision avoidance schemes with control barrier functions [21] for separation. The control input for each rigid body is chosen by solving a distributed optimization problem with constraints for pose synchronization and collision avoidance. A relaxation parameter is introduced to the constraints for position synchronization and is minimized in the optimization to allow the most cohesion within the group as possible without collisions. this letter also provides theoretical guarantees for the cohesion/alignment method and separation one. The effectiveness of the proposed flocking algorithm is demonstrated via simulation and hardware experiments.

II. Problem Formulation

A. Rigid Body Network

Throughout this work, we consider a network of n rigid bodies in 3D space as illustrated in Fig. 1. Let the world frame be Σ_w and body-fixed frames Σ_i, $i \in \mathcal{V} := \{1, \dots, n\}$. The pose of rigid body i relative to Σ_w is denoted by $g_{wi} = (p_{wi}, e^{\hat{\xi}_{wi}\theta_{wi}}) \in SE(3) := \mathbb{R}^3 \times SO(3)$, $SO(3) := \{R \in \mathbb{R}^{3\times 3} \mid RR^{\mathrm{T}} = I_3,\ \det R = 1\}$. ($I_n \in \mathbb{R}^{n\times n}$ is the $n \times n$ identity matrix.) Here, the attitude is given by the exponential coordinate of the rotation matrix $e^{\hat{\xi}\theta} \in SO(3)$ with the rotation axis $\xi \in \mathbb{R}^3$ ($\|\xi\| = 1$) and the angle $\theta \in \mathbb{R}$ [22]. The operator $\wedge : \mathbb{R}^3 \to so(3) := \{S \in \mathbb{R}^{3\times 3} \mid S + S^{\mathrm{T}} = O_3\}$ provides $\hat{a}b = a \times b$ for any 3D vectors $a, b \in \mathbb{R}^3$, and $\vee : so(3) \to \mathbb{R}^3$ is its inverse operator. ($O_n \in \mathbb{R}^{n\times n}$ is the $n \times n$ zero matrix.) For the ease of representation, $\hat{\xi}_{wi}\theta_{wi}$ is written by $\hat{\xi}\theta_{wi}$ in this letter.

The body velocity of rigid body i relative to Σ_w is represented by $V^b_{wi} = [(v^b_{wi})^{\mathrm{T}}\ (\omega^b_{wi})^{\mathrm{T}}]^{\mathrm{T}} \in \mathbb{R}^6$, where $v^b_{wi}, \omega^b_{wi} \in \mathbb{R}^3$ are the translational and angular body velocity, respectively. The pose g and body velocity V^b can be written by the following homogeneous representation:

$$g = \begin{bmatrix} e^{\hat{\xi}\theta} & p \\ 0 & 1 \end{bmatrix} \in \mathbb{R}^{4\times 4}, \hat{V}^b = \begin{bmatrix} \hat{\omega} & v \\ 0 & 0 \end{bmatrix} \in \mathbb{R}^{4\times 4}.$$

In this formulation, the body velocity is given by $\hat{V}^b_{wi} = g^{-1}_{wi}\dot{g}_{wi}$, which provides the following *rigid body motion* as the motion dynamics of each rigid body $i \in \mathcal{V}$ [22]:

$$\dot{g}_{wi} = g_{wi}\hat{V}^b_{wi}. \tag{1}$$

This work considers the body velocity V^b_{wi}, viewed from Σ_i, as the control input of rigid body i.

The interconnection topology between rigid bodies is represented by an undirected graph $\mathcal{G} = (\mathcal{V}, \mathcal{E})$ [23], where $\mathcal{V}$ is the set of rigid bodies and $\mathcal{E} \subset \mathcal{V} \times \mathcal{V}$ the edge set defining information flow between rigid bodies. Then, the neighbor set of rigid body i is defined as $\mathcal{N}_i := \{j \in \mathcal{V} \mid (j, i) \in \mathcal{E}\}$, which is analogous to rigid body i obtaining information about rigid body j if $j \in \mathcal{N}_i$. Since this work considers undirected information flow, $j \in \mathcal{N}_i \Leftrightarrow i \in \mathcal{N}_j$ holds.

In the subsequent discussion, a group of n rigid bodies with rigid body motion (1) and the interconnection topology $\mathcal{G}$ is called a *Rigid Body Network*.

B. Control Objective

The goal of this work is to propose a distributed flocking algorithm embodying Reynolds's flocking rules: cohesion; alignment; and separation, while explicitly dealing with the conflict between cohesion and separation. To formulate this objective, let us first introduce the relative pose of rigid body j with respect to rigid body i defined as $g_{ij} := g^{-1}_{wi}g_{wj} = (p_{ij}, e^{\hat{\xi}\theta_{ij}}) \in SE(3)$.

This work imposes the information restriction that only the relative poses g_{ij} with respect to neighboring rigid bodies $j \in \mathcal{N}_i$ (and neighbors for separation) are available for the control input V^b_{wi} of each rigid body $i \in \mathcal{V}$. This restriction enables each rigid body to implement the control law only by its own relative sensing device, i.e., as a fully distributed system as in [24], [25].

Let us now define the control objective. Since the flocking rules have an inherent conflict between cohesion and separation, these objectives are first considered separately. The cohesion and alignment objectives can be considered as pose synchronization whose definition is given as follows:

Definition 1: The rigid body network is said to achieve *pose synchronization* if

$$\lim_{t\to\infty} \|p_{ij}(t)\| = 0 \ \forall\, i, j \in \mathcal{V}, \tag{2a}$$

$$\lim_{t\to\infty} \phi(e^{\hat{\xi}\theta_{ij}}(t)) = 0 \ \forall\, i, j \in \mathcal{V}, \tag{2b}$$

where, $\phi(e^{\hat{\xi}\theta}) := \|\log(e^{\hat{\xi}\theta})^{\vee}\|^2 \geq 0$ is the scalar function to indicate the attitude error from the origin: $\phi(I_3) = 0$ [26].

Equation (2) is only satisfied when the poses of all rigid bodies converge to a common one, i.e., cohesion and alignment are achieved (see Fig. 2(a)). Individual equalities (2a) and (2b) describe position and attitude requirements which are also referred to as *position synchronization* and *attitude synchronization*, respectively. Here, position synchronization (2a) is just a theoretical aspiration, i.e., not actually achieved in a physical system, to make it easy to understand the concept of cohesion.

Beyond the pose synchronization, successful flocking of rigid bodies additionally requires a separation behavior. Collisions between rigid bodies and collision avoidance in the rigid body network are defined as follows (see Fig. 2(b)):

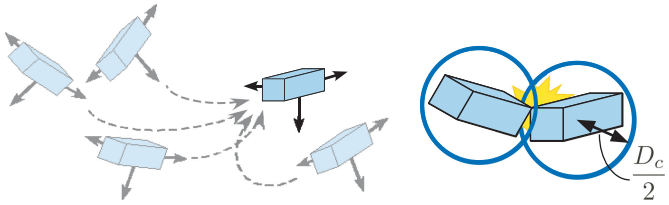

(a) Pose synchronization. (b) Collision.

Fig. 2. Cartoon representation of (a) pose synchronization and (b) collision. (a): All rigid bodies converge to the same position and attitude. (b): The distance between rigid bodies is less than their diameter D_c.

Definition 2: Rigid body i and rigid body j are said to collide with each other if

$$\|p_{wi} - p_{wj}\| < D_c,$$

where $D_c > 0$ is the collision distance. Then, the rigid body network is said to achieve *collision avoidance* if

$$\|p_{wi}(t) - p_{wj}(t)\| \geq D_c \ \forall\, i, j \in \mathcal{V}(i \neq j), t \geq 0. \quad (3)$$

By defining the following set for the rigid body network:

$$C := \{p_{wi},\, i \in \mathcal{V} \mid \|p_{wi} - p_{wj}\| \geq D_c \ \forall\, i, j \in \mathcal{V}(i \neq j)\}, \quad (4)$$

collision avoidance (3) is analogous to the forward invariance of the set C. Notice here that collision avoidance (3) must be guaranteed over position synchronization (2) in practice as collisions can damage or destroy individuals within the collective.

In summary, the control objective of the rigid body network is to achieve the following three requirements according to the flocking rules:

(i) position synchronization (2a) as much as possible;
(ii) attitude synchronization (2b);
(iii) collision avoidance (3).

C. Proposed Optimization Approach

In order to handle control objective (i) explicitly, this work employs the following type of optimization problem for each rigid body $i \in \mathcal{V}$ in the rigid body network:

$$\min_{V^b_{wi} \in \mathbb{R}^6, \delta_i \in \mathbb{R}} (V^b_{wi})^{\mathrm{T}} V^b_{wi} + \delta_i^2$$
$$\text{s.t. Objectives (i), (ii), and (iii) are achieved.} \quad (5)$$

In this optimization formulation, the achievement of the flocking motion is managed by constraints. Here, the relaxation parameter $\delta_i \in \mathbb{R}$ is introduced to the constraint for objective (i) since we aim to achieve position synchronization (2a) *as much as possible*. (The formal definition of δ_i is provided in Section III-C.) In other words, δ_i manages the inherent conflict between position synchronization (2a) and collision avoidance (3). Then, minimizing δ_i^2 in this optimization problem implies achieving objective (i). We also introduce the quadratic form of the control input V^b_{wi} to the cost function in order to avoid undesired input excitation and save input energy.[1]

The constraints for pose synchronization (2) and collision avoidance (3) are further developed in Section III.

[1]We can also apply a positive weight to δ_i^2 in order to tune the importance of its minimization compared with $\|V^b_{wi}\|^2$.

D. Review of Control Barrier Functions for Collision Avoidance and Their Application to Quadratic Programs

As the preliminary of this work, let us briefly introduce a notion of a control barrier function (CBF) and its application to a control method based on a quadratic program (QP) (see [21] for more details). Consider the system

$$\dot{x} = f(x) + g(x)u,\ x \in \mathbb{R}^m,\ u \in \mathbb{R}^l$$

and a task to ensure the forward invariance of the set

$$C_o = \{x \in \mathbb{R}^m \mid H(x) \geq 0\}.$$

Here, $f : \mathbb{R}^m \to \mathbb{R}^m$ and $g : \mathbb{R}^m \to \mathbb{R}^{m \times l}$ are locally Lipschitz, and $H : \mathbb{R}^m \to \mathbb{R}$ is a continuously differentiable function.

For this task, a zeroing CBF is defined as follows:

Definition 3. ([21]): The function H is said to be a *Zeroing Control Barrier Function (ZCBF)* for the set C_o if there exists an extended class $\mathcal{K}$ function $\alpha : \mathbb{R} \to \mathbb{R}$ such that

$$\sup_{u \in \mathbb{R}^l} \left(\dot{H}(x) + \alpha\left(H(x)\right) \right) \geq 0.$$

Then, the following fact holds:

Fact 1: ([21]) If the function H is a ZCBF for the set C_o, then any Lipschitz continuous controller u satisfying

$$\mathcal{L}_f H(x) + \mathcal{L}_g H(x) u + \alpha(H(x)) \geq 0 \quad (6)$$

will render the set C_o forward invariant. Here, $\mathcal{L}_f$ and $\mathcal{L}_g$ are the Lie derivatives along f and g, respectively.

Condition (6) is called the *ZCBF condition* in this letter. Then, this work designs ZCBFs and derives ZCBF conditions, based only on relative pose information with respect to neighboring rigid bodies, for each rigid body to avoid collisions.

The work [21] also proposes a Lyapunov-based control approach with a guarantee of the forward invariance of C_o by a CBF. Suppose that the control objective (task) is given by a control Lyapunov function $U_o \geq 0$, i.e., the control objective is $\lim_{t \to \infty} U_o(t) = 0$. This can be achieved by choosing a Lipschitz continuous controller u satisfying

$$\mathcal{L}_f U_o(x) + \mathcal{L}_g U_o(x) u + c U_o(x) \leq 0,\ c > 0. \quad (7)$$

Then, by taking the possibility of the conflict between (6) and (7) into consideration, the authors in [21] present the following control input given by a solution of a QP to guarantee the forward invariance of the set C_o and to achieve the control objective as much as possible:

$$u^* = \arg \min_{u \in \mathbb{R}^l,\ \delta \in \mathbb{R}} u^{\mathrm{T}} u + \delta^2$$
$$\text{s.t. } \mathcal{L}_f H(x) + \mathcal{L}_g H(x) u + \alpha(H(x)) \geq 0,$$
$$\mathcal{L}_f U_o(x) + \mathcal{L}_g U_o(x) u + c U_o(x) - \delta \leq 0.$$

Here, condition (7) for the control objective is relaxed by δ to manage the conflict.

This work employs this optimization technique for the achievement of the flocking behavior, where the collision avoidance is handled by constraint (6) and the relaxed pose synchronization is incorporated through constraint (7).

III. Optimization-Based Flocking Control

A. ZCBF Conditions for Collision Avoidance

Let us first consider ZCBFs for collision avoidance (3), i.e., separation. Notice that it is sufficient for each rigid body to avoid collisions only when it is near others. Therefore, in addition to the graph $\mathcal{G}$ for the pose synchronization, we introduce another distance-based graph $\mathcal{G}' = (\mathcal{V}, \mathcal{E}')$, $\mathcal{E}' := \{(i,j) \in \mathcal{V}(i \neq j) \mid \|p_{ij}\| \leq D_a \ \forall\, i,j \in \mathcal{V}\}$ that is often called a Δ-disk proximity graph [23]. Here, $D_a > D_c$ is the distance within which rigid bodies take separation behaviors into consideration. Then, a new neighbor set of rigid body i for the collision avoidance, referred to as *distance neighbors*, is defined as $\mathcal{N}_{di} := \{j \in \mathcal{V} \mid (j,i) \in \mathcal{E}'\}$.

By defining the ZCBF candidates as $H_{ij} := \|p_{wi} - p_{wj}\|^2 - D_c^2 \in \mathbb{R}$ for $i,j \in \mathcal{V}$ and rewriting (4) as

$$C = \{p_{wi},\ i \in \mathcal{V} \mid H_{ij} \geq 0 \ \forall\, i,j \in \mathcal{V}(i \neq j)\},$$

the forward invariance of the set C for the rigid body network guarantees collision free motions for all time. Then, based on Fact 1, we have the following theorem indicating the achievement of collision avoidance (3):

Theorem 1: Let the initial positions of the rigid body network satisfy $\{p_{wi}(0)\}_{i\in\mathcal{V}} \in C$. Then, the set C is forward invariant if v_{wi}^b is chosen to be Lipschitz continuous and satisfy the following condition for each rigid body $i \in \mathcal{V}$:

$$p_{ij}^{\mathrm{T}} v_{wi}^b \leq k_c(\|p_{ij}\|^2 - D_c^2) \ \forall\, j \in \mathcal{N}_{di},\ k_c > 0. \tag{8}$$

Proof: Based on (6) in Fact 1, we first obtain the following ZCBF condition for rigid body i by differentiating H_{ij} with respect to time for rigid body $j \in \mathcal{N}_{di}$:

$$2(p_{wi} - p_{wj})^{\mathrm{T}}(\dot{p}_{wi} - \dot{p}_{wj}) \geq -4k_c(\|p_{wi} - p_{wj}\|^2 - D_c^2) \quad \forall\, j \in \mathcal{N}_{di}. \tag{9}$$

Here, we employ the extended class $\mathcal{K}$ function $\alpha(H) = 4k_cH$ with $k_c > 0$,[2] and note that only the distance neighbors $j \in \mathcal{N}_{di}$ are considered here since $H_{ij} > 0$ holds for any $j \in \mathcal{V} \setminus \mathcal{N}_{di}$ $(j \neq i)$ from $D_a > D_c$. Rigid body motion (1) and the relative pose definition allow condition (9) to be rewritten using relative pose information as follows:

$$-p_{ij}^{\mathrm{T}} v_{wi}^b - p_{ji}^{\mathrm{T}} v_{wj}^b \geq -2k_c(\|p_{ij}\|^2 - D_c^2) \ \forall\, j \in \mathcal{N}_{di}. \tag{10}$$

Notice, however, that condition (10) is not distributed, i.e., if rigid body i tries to satisfy (10), input information of its distance neighbors and its own relative positions viewed from those neighbors are necessary. Therefore, we consider distributed condition (8) to satisfy (10). Then, since $j \in \mathcal{N}_{di} \Leftrightarrow i \in \mathcal{N}_{dj}$ holds, satisfying (8) for all $i \in \mathcal{V}$ results in the satisfaction of (10), i.e., (9), for all $i \in \mathcal{V}$. Here, replacing (10) with (8) can be interpreted as sharing condition (10) equally,[3] between rigid body i and rigid body j. Fact 1 thus concludes the forward invariance of the set C. ■

This work employs condition (8) as the constraint for control objective (iii) by the QP presented in (5).

[2]Any extended class $\mathcal{K}$ functions can be employed as $\alpha(H)$, e.g., $\alpha(H) = \gamma H^3$, $\gamma > 0$. It is usually selected in view of control requirements and the existence of solutions of the resulting QPs.

[3]It is also possible to employ weights w_{ij} $(j,i) \in \mathcal{E}'$ such that $w_{ij} + w_{ji} = 1$ for sharing condition (10) between rigid body i and rigid body j.

Remark 1: ZCBF condition (8), for each rigid body i, is distributed since it is based only on information about its distance neighbors $j \in \mathcal{N}_{di}$. Condition (8) is also based only on relative position information p_{ij} viewed from Σ_i.

B. Conditions for Pose Synchronization

We next derive conditions for pose synchronization (2), i.e., cohesion and alignment. Consider the following conditions on the body velocity input V_{wi}^b for each rigid body $i \in \mathcal{V}$:

$$\sum_{j\in\mathcal{N}_i} p_{ij}^{\mathrm{T}} v_{wi}^b \geq k_p \left\| \sum_{j\in\mathcal{N}_i} p_{ij} \right\|^2, \tag{11}$$

$$\sum_{j\in\mathcal{N}_i} (\log(e^{\hat{\xi}\theta_{ij}})^{\vee})^{\mathrm{T}} \omega_{wi}^b \geq k_e \left\| \sum_{j\in\mathcal{N}_i} \log(e^{\hat{\xi}\theta_{ij}})^{\vee} \right\|^2. \tag{12}$$

Here, $k_p, k_e > 0$ are gains.

Condition (11) for position synchronization (2a) can be rewritten as

$$\frac{\sum_{j\in\mathcal{N}_i} p_{ij}^{\mathrm{T}}}{\|\sum_{j\in\mathcal{N}_i} p_{ij}\|} v_{wi}^b \geq k_p \left\| \sum_{j\in\mathcal{N}_i} p_{ij} \right\| \geq 0$$

when $\sum_{j\in\mathcal{N}_i} p_{ij} \neq 0$. This means that the inner product of the input v_{wi}^b and a unit vector toward the centroid of the relative positions on $\mathcal{N}_i$ viewed from Σ_i is not negative, that is, the direction of the translational velocity is chosen to approach the centroid. The size of the input v_{wi}^b is based on the distance to the centroid multiplied by k_p, i.e., k_p has a gain-like effect to regulate the produced velocity. This behavior eventually achieves position synchronization (2a) as shown in the next theorem. Condition (12) for attitude synchronization (2b) can be interpreted similarly since $\log(e^{\hat{\xi}\theta})^{\vee} = \xi\theta$ holds for $|\theta| < \pi$, i.e., its direction is equivalent to the rotation axis [26], and attitude synchronization (2b) can be regarded as the synchronization of the rotation axes and angles.

Then, we have the following theorem indicating the achievement of pose synchronization (2):

Theorem 2: Suppose that the interconnection topology $\mathcal{G}$ in the rigid body network is fixed and connected, and the attitudes satisfy $|\theta_{ij}(t)| < \pi$ for all $i,j \in \mathcal{V}$, $t \geq 0$. Then, pose synchronization (2) is achieved if V_{wi}^b is chosen to be Lipschitz continuous and satisfy conditions (11) and (12) for all $i \in \mathcal{V}$.

Proof: See Appendix. ■

This work employs condition (12) as the constraint for control objective (ii) by the QP presented in (5).

Remark 2: Conditions (11) and (12) are also distributed, i.e., based only on information about $\mathcal{N}_i$, and built by relative pose information g_{ij} viewed from Σ_i. Although the assumption $|\theta_{ij}(t)| < \pi\ \forall\, i,j \in \mathcal{V},\ t \geq 0$ seems to be restrictive, it can be relaxed to be the initial attitude condition, which is given in the next section.

C. Flocking Algorithm

The final flocking algorithm combines the QP constraints developed in Sections III-A and III-B. These constraints cannot be applied simultaneously in their current form since position synchronization (2a) and collision avoidance (3) (i.e., cohesion and separation) cannot be achieved at the same time. When applying this kind of flocking control to a multi-robot system,

collision avoidance must be achieved to avoid potential damage of individuals within the collective. We thus relax condition (11) by introducing $\delta_i \geq 0$ as follows:

$$\sum_{j\in\mathcal{N}_i} p_{ij}^{\mathrm{T}} v_{wi}^b \geq k_p \left\| \sum_{j\in\mathcal{N}_i} p_{ij} \right\|^2 - \delta_i. \tag{13}$$

This work employs condition (13) as the constraint for control objective (i) by the QP presented in (5).

In summary, for each rigid body $i \in \mathcal{V}$ in the rigid body network, we propose the following flocking control input given by the solution of the QP in (5) with (8), (12), and (13):

$$\begin{aligned} V_i^* = \arg \min_{V_{wi}^b\in\mathbb{R}^6,\ \delta_i\geq 0} & (V_{wi}^b)^{\mathrm{T}} V_{wi}^b + \delta_i^2 \\ \text{s.t.} \sum_{j\in\mathcal{N}_i} p_{ij}^{\mathrm{T}} v_{wi}^b &\geq k_p \left\| \sum_{j\in\mathcal{N}_i} p_{ij} \right\|^2 - \delta_i, \\ \sum_{j\in\mathcal{N}_i} (\log(e^{\hat{\xi}\theta_{ij}})^\vee)^{\mathrm{T}} \omega_{wi}^b &\geq k_e \left\| \sum_{j\in\mathcal{N}_i} \log(e^{\hat{\xi}\theta_{ij}})^\vee \right\|^2, \\ p_{ij}^{\mathrm{T}} v_{wi}^b &\leq k_c(\|p_{ij}\|^2 - D_c^2)\ \forall\ j \in \mathcal{N}_{di}. \end{aligned} \tag{14}$$

The optimization in (14) is feasible in the collision avoidance set C, thanks to the QP formulation with the relaxation parameter δ_i, which provides a unique optimal solution in the sense of the minimization of both $\|V_{wi}^b\|$ and δ_i. As stated in Section II-C, the minimization of $\|V_{wi}^b\|$ can be considered as attenuating undesired input excitation and saving energy, while minimizing δ_i aims to achieve position synchronization (2a) as much as possible while maintaining safe distances between all rigid bodies to avoid collisions.

For the proposed flocking algorithm (14), we have the following theorem:

Theorem 3: If the initial poses of the rigid body network satisfy $\{p_{wi}(0)\}_{i\in\mathcal{V}} \in C$, $|\theta_{ij}(0)| < \pi\ \forall\ i, j \in \mathcal{V}$ and the interconnection topology $\mathcal{G}$ is fixed and connected, then flocking algorithm (14) achieves attitude synchronization (2b) and collision avoidance (3).

Proof: See Appendix. ■

Theorem 3 guarantees the achievement of alignment and separation. Moreover, since minimizing δ_i^2 implies to achieve condition (11) as much as possible, we can also expect the achievement of the most cohesion as possible while respecting the necessary separation distances for safety.

Remark 3: The proposed flocking algorithm (14) is fully distributed. This feature enables each rigid body to implement its control input by using only local sensors. Another advantage of the present approach is the ease of incorporating other functions for the rigid body network by additionally imposing constraints for, e.g., connectivity maintenance [29] and input limitations. Especially, we can easily introduce translational velocity input saturation, e.g., $\|v_{wi}^b\| \leq v_{\max}$ for some $v_{\max} > 0$, since at least $v_{wi}^b = 0$ satisfies the constraints in (14) for bounded relative positions $p_{ij},\ j \in \mathcal{N}_i$.

D. Flocking With Desired Behavior

So far we have shown that flocking algorithm (14) captures all three requirements: cohesion; alignment; and separation. However, the rigid body network will stop after the achievement of the flocking behavior by this method. This is not suited to some situations, e.g., the network must move through an area. We thus provide an extension of the present algorithm to move in a desired direction.

Suppose that there exists a beacon, e.g., tower or mountain, in Σ_w, and all rigid bodies in the network have common translational velocity $v_d \in \mathbb{R}^3$ to move toward it. Then, by introducing the rotation matrix $e^{\hat{\xi}\theta_{wb}} \in SO(3)$ to represent the direction of v_d to the beacon in Σ_w, we can modify the translational velocity input given by (14) as follows:

$$v_{wi}^b = v_i^* + e^{\hat{\xi}\theta_{ib}} v_d,\ i \in \mathcal{V}. \tag{15}$$

Here, $v_i^* \in \mathbb{R}^3$ is the translational component of V_i^* in (14).

Notice now that the additional term is also formed by the relative information with respect to the beacon because of $e^{\hat{\xi}\theta_{ib}} v_d = e^{-\hat{\xi}\theta_{wi}} e^{\hat{\xi}\theta_{wb}} v_d$ that points the direction to the beacon viewed from Σ_i. We also note that the velocity modification of (15) does not affect the time derivative of the term $\|p_{wi} - p_{wj}\|^2$. This means that the time evolution of relative poses does not change, that is, even with the velocity modification of (15), the same flocking behavior as (14) is achieved. If necessary, common angular velocity $\omega_d \in \mathbb{R}^3$ can be also introduced as $\omega_{wi}^b = \omega_i^* + e^{\hat{\xi}\theta_{ib}}\omega_d$ because $\dot{\phi}(e^{\hat{\xi}\theta_{ij}})$ does not change due to this modification.

IV. Experimental Results

A. Simulation

3D simulation is first conducted to demonstrate the proposed fully distributed flocking algorithm (14), (15). Consider the rigid body network with 30 rigid bodies. The interconnection topology between rigid bodies is given as a cyclic undirected graph $\mathcal{G}$, i.e., $\mathcal{N}_i = \{i-1,\ i+1\}$ for $i \in \{2, \ldots, 29\}$, $\mathcal{N}_1 = \{30, 2\}$, and $\mathcal{N}_{30} = \{29, 1\}$. Let the initial poses $g_{wi}(0),\ i \in \mathcal{V}$ be randomly set such that $p_{wi}(0) \in [-50, 50]^3$ [m]^3 and $\theta_{wi}(0) \in (-\pi/2, \pi/2)$ [rad] that satisfies the initial attitude condition of Theorem 3. Then, flocking algorithm (14), (15) developed in this letter, with $k_p = 2$, $k_e = 3$, $k_c = 0.5$, $D_c = 0.5$ [m], $D_a = 5$ [m], and $e^{\hat{\xi}\theta_{wb}} v_d = [2.5\ 2.5\ 2.5]^{\mathrm{T}}$ [m/s], is applied to each rigid body in the rigid body network.

The simulation results are provided in Fig. 3. Fig. 3(a) depicts the 3D position trajectories of the rigid body network in Σ_w, which demonstrates the proposed controller achieves the desired cohesion behavior with movement in the desired direction. Fig. 3(b) illustrates the time responses of the attitude angles around x- (red), y- (green), and z- (blue) axes in Σ_w. This figure shows the achievement of the attitude synchronization, i.e., the desired alignment behavior. We finally provide the time responses of the maximum (minimum) relative distance between rigid body pairs connected by the edges of $\mathcal{G}$ ($\mathcal{G}'$) in Fig. 3(c). This figure shows that the minimum relative distance never reaches the collision distance D_c, i.e., the achievement of the desired separation behavior. The decrease of the maximum relative distance, starting from 123.3 m, also shows the achievement of the desired cohesion behavior.

In summary, the proposed flocking algorithm (14), (15) successfully achieves the desired cohesion, alignment, and separation behaviors for the rigid body network.

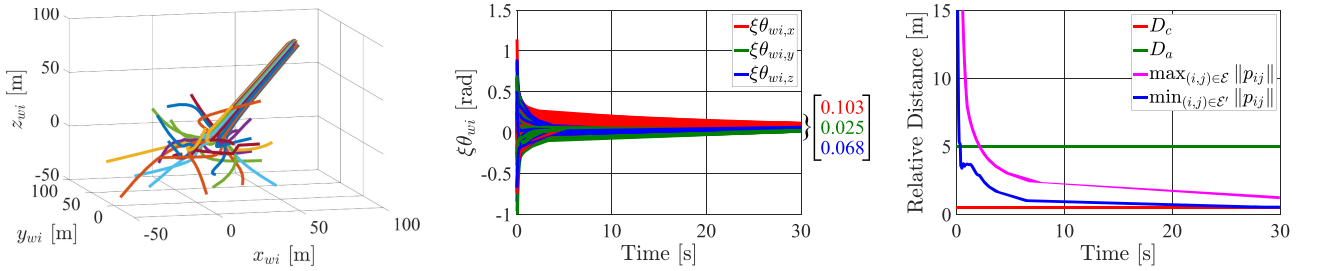

(a) 3D position trajectories in Σ_w. (b) Time responses of 3D attitudes in Σ_w. (c) Time responses of maximum/minimum relative distances.

Fig. 3. Simulation results. (a): The rigid body network achieves the cohesion behavior and moves in the desired direction. (b): Red, green, and blue lines represent the attitudes of all rigid bodies around $x-$, $y-$, and $z-$axes in Σ_w. All the angles of each axis converge to a common one, i.e., the achievement of the alignment behavior. (c): The minimum relative distance never reaches the collision distance D_c, i.e., the achievement of the separation behavior. The decrease of the maximum relative distance, starting from 123.3 m, also shows the achievement of the cohesion behavior.

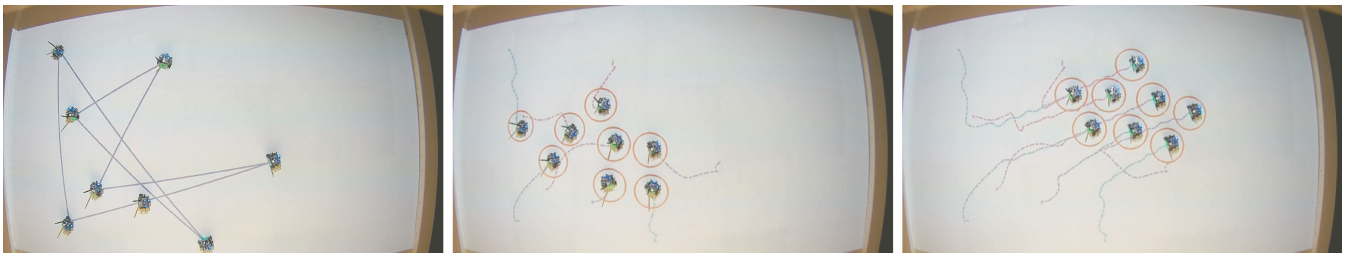

(a) $t = 0$ [s]. (b) $t = 10$ [s]. (c) $t = 50$ [s].

Fig. 4. Snapshots of experiment at (a) $t = 0$ [s]; (b) $t = 10$ [s]; and (c) $t = 50$ [s]. (a): The blue lines show the interconnection topology between the vehicles. (b): The red circles and dotted lines represent the half of the collision distances and the trajectories, respectively. The cohesion behavior is first almost achieved while guaranteeing the separation one. (c): The alignment behavior and movement in the desired direction are finally achieved.

B. Experimental Environment

The proposed flocking algorithm (14), (15) is validated on the Robotarium, a remotely accessible swarm robotics testbed [30]. The Robotarium enables users around the world to control small differential-drive robots through code scripts uploaded via a web interface. The pose data presented in this section is tracking data from the Vicon motion capture system [31] mounted above the Robotarium testbed. The controllable robots in the Robotarium are ground two-wheeled vehicles with a nonholonomic constraint [22], i.e., the vehicles cannot move in the side direction. Therefore, we demonstrate the effectiveness of the proposed algorithm as a top level controller, that is, the algorithm provides reference inputs and a local controller attempts to track the virtual trajectory generated by the reference inputs.

The 3D pose $g_{wi} \in SE(3)$ is first reduced to the 2D one $\tilde{g}_{wi} = (\tilde{p}_{wi},\ e^{\hat{1}\theta_{wi}}) \in SE(2) := \mathbb{R}^2 \times SO(2)$ as follows:

$$\tilde{g}_{wi} = \begin{bmatrix} e^{\hat{1}\theta_{wi}} & \tilde{p}_{wi} \\ 0 & 1 \end{bmatrix} \in \mathbb{R}^{3\times 3},\ \hat{\tilde{V}}^b_{wi} = \begin{bmatrix} \hat{\tilde{\omega}}^b_{wi} & \tilde{v}^b_{wi} \\ 0 & 0 \end{bmatrix} \in \mathbb{R}^{3\times 3}.$$

Here, the operator '$\wedge$' for a scalar value provides a matrix on $so(2)$ [22]. We note that even with this 2D model, the same results as in Section III-C can be obtained.

This $SE(2)$ model has the 2D translational velocity input $\tilde{v}^b_{wi}$, but due to the motion constraints, the actual vehicle testbed can generate only 1D longitudinal velocity. We thus employ the pose regulation law for two-wheeled vehicles presented in [32] as the local controller, and flocking algorithm (14), (15) is utilized as the top level controller to generate the desired pose for the local one. Here, we calculate the desired pose with the pose transition by supposing that the top level controller input is applied for some time interval $T > 0$.

C. Results

The parameters of the proposed flocking algorithm (14), (15) are set as $k_p = 5$, $k_e = 3$, $k_c = 3$, $D_c = 0.3$ [m], $D_a = 0.5$ [m], $e^{\hat{1}\theta_{wb}} v_d = [0.18\ 0.08]^{\mathrm{T}}$ [m/s], and $T = 0.2$ [s]. Here, we set a larger value for D_c than the diameter of the robots since the actual velocity input generated by the local controller is different from that of the original flocking controller. The rigid body network consists of 8 robots and a cyclic undirected graph $\mathcal{G}$.

The experimental results are provided in Figs. 4 and 5. The snapshots of the experiment at $t = 0$ [s], $t = 10$ [s], and $t = 50$ [s] are shown in Fig. 4. Figs. 5(a) and 5(c) show that the rigid body network achieves the cohesion and separation behaviors successfully. During the experiment, the minimum relative distance between the vehicles becomes lower than D_c sporadically but never more than 2 cm. This can be attributed to the differential drive motion constraints of the platform and tracking error. However, by making D_c slightly larger than the diameter of the physical platform, these application complexities do not cause physical collisions of the robots. Fig. 5(b) also shows that the alignment behavior is almost achieved. Due to the differential drive constraints of the robots, the attitude synchronization takes longer and some oscillation appears in this implementation, but after the position synchronization is nearly achieved, the network achieves the attitude consensus as well.

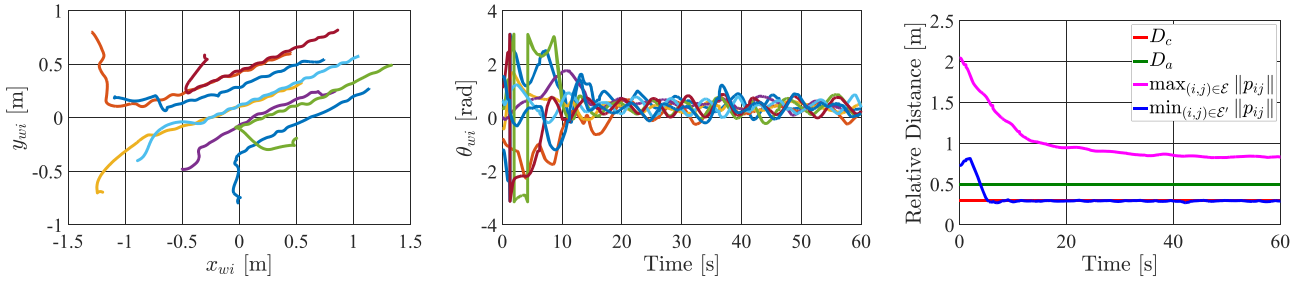

(a) 2D position trajectories in Σ_w.

(b) Time responses of 1D attitudes in Σ_w.

(c) Time responses of maximum/minimum relative distances.

Fig. 5. Experimental results. (a): The rigid body network achieves the cohesion behavior and moves in the desired direction. (b): Due to the differential drive constraints of the robots, the attitude synchronization takes longer and some oscillation appears in this implementation, but after the position synchronization is nearly achieved, the network achieves the attitude consensus as well. (c): The minimum relative distance between the vehicles becomes lower than D_c sporadically but never more than 2 cm, which does not cause physical collisions of the robots.

In summary, the proposed flocking algorithm (14), (15) works well as a top level controller.

V. Conclusion

This letter presented a distributed 3D flocking control algorithm for networked rigid bodies. The proposed method captures Reynolds's three fundamental flocking rules: cohesion; alignment; and separation, and can be implemented by each rigid body as a fully distributed system. The present problem formulation handles the conflict between cohesion and separation in optimization problems with relaxation parameters for cohesion constraints. This letter also provided theoretical guarantees for cohesion/alignment and separation methods. The effectiveness of the proposed flocking algorithm has been validated via 3D simulation and also demonstrated as a high level controller through 2D experiments.

Appendix

A. Proof of Theorem 2

Proof: Define the potential function $U := U_p + U_a \geq 0$,

$$U_p := \frac{1}{4k_p}\sum_{i\in\mathcal{V}}\sum_{j\in\mathcal{N}_i}\|p_{wi}-p_{wj}\|^2 \geq 0,$$

$$U_a := \frac{1}{2k_e}\sum_{i\in\mathcal{V}}\sum_{j\in\mathcal{N}_i}\phi(e^{\hat{\xi}\theta_{ij}}) \geq 0.$$

Then, the time derivative of U_p yields

$$\dot{U}_p = \frac{1}{2k_p}\sum_{i\in\mathcal{V}}\sum_{j\in\mathcal{N}_i}(p_{wi}-p_{wj})^{\mathrm{T}}(\dot{p}_{wi}-\dot{p}_{wj})$$

$$= \frac{1}{k_p}\sum_{i\in\mathcal{V}}\sum_{j\in\mathcal{N}_i}(p_{wi}-p_{wj})^{\mathrm{T}}\dot{p}_{wi}, \tag{16}$$

where the second equality is given by the connectivity of the interconnection topology $\mathcal{G}$, i.e., $j\in\mathcal{N}_i \Leftrightarrow i\in\mathcal{N}_j$. Rigid body motion (1) and the relative pose definition can rewrite (16) using the relative positions and velocity inputs as

$$\dot{U}_p = -\frac{1}{k_p}\sum_{i\in\mathcal{V}}\sum_{j\in\mathcal{N}_i}p_{ij}^{\mathrm{T}}v_{wi}^b.$$

Therefore, satisfying condition (11) for all $i\in\mathcal{V}$ yields

$$\dot{U}_p \leq -\sum_{i\in\mathcal{V}}\left\|\sum_{j\in\mathcal{N}_i}p_{ij}\right\|^2 \leq 0.$$

Similarly to (16), the time derivative of U_a provides

$$\dot{U}_a = -\frac{1}{k_e}\sum_{i\in\mathcal{V}}\sum_{j\in\mathcal{N}_i}(\log(e^{\hat{\xi}\theta_{ij}})^\vee)^{\mathrm{T}}\omega_{wi}^b.$$

Here, we utilize the properties on the logarithmic map[4]: $\dot{\phi}(e^{\hat{\xi}\theta}) = (\log(e^{\hat{\xi}\theta})^\vee)^{\mathrm{T}}\omega^b$; $e^{\hat{\xi}\theta}\log(e^{\hat{\xi}\theta})^\vee = \log(e^{\hat{\xi}\theta})^\vee$; and $\log(e^{-\hat{\xi}\theta}) = -\log(e^{\hat{\xi}\theta})$, and the connectivity of $\mathcal{G}$. Therefore, the satisfaction of condition (12) for all $i\in\mathcal{V}$ yields

$$\dot{U}_a \leq -\sum_{i\in\mathcal{V}}\left\|\sum_{j\in\mathcal{N}_i}\log(e^{\hat{\xi}\theta_{ij}})^\vee\right\|^2 \leq 0.$$

In summary, we obtain

$$\dot{U} \leq -\sum_{i\in\mathcal{V}}\left\|\sum_{j\in\mathcal{N}_i}p_{ij}\right\|^2 - \sum_{i\in\mathcal{V}}\left\|\sum_{j\in\mathcal{N}_i}\log(e^{\hat{\xi}\theta_{ij}})^\vee\right\|^2 \leq 0.$$

Since V_{wi}^b is chosen to be Lipschitz continuous, the LaSalle's Invariance Principle [27] can be applied to the convergence analysis. Then, from the properties that $\log(e^{\hat{\xi}\theta})^\vee$ is bijective for $|\theta|<\pi$; $\log(e^{\hat{\xi}\theta})^\vee = 0 \Leftrightarrow e^{\hat{\xi}\theta} = I_3$; $|\theta_{ij}(t)|<\pi\ \forall\, i,j\in\mathcal{V}$, $t\geq 0$; and $\mathcal{G}$ is connected, $\dot{U}=0$ is equivalent to pose synchronization (2), which concludes the proof. ■

B. Proof of Theorem 3

Proof: Notice first that the attitude components of rigid body motion (1) and the QP in (14) are independent of the position ones. We thus obtain the following attitude synchronization input from the Karush-Kuhn-Tucker condition [28]:

$$\omega_{wi}^b = k_e\sum_{j\in\mathcal{N}_i}\log(e^{\hat{\xi}\theta_{ij}})^\vee. \tag{17}$$

Since this input satisfies condition (12) and collision avoidance condition (8) is used in the QP in (14), attitude synchronization

[4]Refer to [26] for the first property. The second and third properties can be confirmed by direct calculations.

(2b) and collision avoidance (3) are guaranteed if $|\theta_{ij}(t)| < \pi \ \forall \ i, j \in \mathcal{V}$ is satisfied for all time $t \geq 0$.

This attitude property is proved by the same technique as Lemma 9.2 in [19]. We first note that the condition $|\theta_{ij}(t)| < \pi \ \forall \ i, j \in \mathcal{V}$ is equivalent to the existence of $\theta_c \in \mathbb{R}$ such that $|\theta_{wi}(t) - \theta_c| < \pi/2 \ \forall \ i \in \mathcal{V}$. Therefore, without loss of generality, we show $|\theta_{wi}(t)| < \pi/2 \ \forall \ i \in \mathcal{V}, \ t > 0$ under the initial condition $|\theta_{wi}(0)| < \pi/2 \ \forall \ i \in \mathcal{V}$. Notice also that $\phi(e^{\hat{\xi}\theta}) = |\theta|^2$ holds for $|\theta| < \pi$ [26]. Then, by denoting the rigid body whose rotation angle is the largest by $\beta(t) \in \mathcal{V}$, it is sufficient for the proof to show that $\phi(e^{\hat{\xi}\theta_{w\beta(t)}})$ does not increase with respect to time in the region $|\theta_{w\beta(t)}| < \pi/2$.

The time derivative of $\phi(e^{\hat{\xi}\theta_{w\beta}})$ along the trajectories of (1) and (17) yields

$$\begin{aligned}\dot{\phi}(e^{\hat{\xi}\theta_{w\beta}}) &= (\log(e^{\hat{\xi}\theta_{w\beta}})^{\vee})^{\mathrm{T}}\omega^b_{w\beta} \\ &= k_e \sum_{j\in\mathcal{N}_\beta} \frac{\theta_{w\beta}}{\sin\theta_{w\beta}} \frac{\theta_{\beta j}}{\sin\theta_{\beta j}} (\mathrm{sk}(e^{\hat{\xi}\theta_{w\beta}})^{\vee})^{\mathrm{T}} \mathrm{sk}(e^{\hat{\xi}\theta_{\beta j}})^{\vee}.\end{aligned}$$

Here, we use the property on the logarithmic map: $\log(e^{\hat{\xi}\theta})^{\vee} = (\theta/\sin\theta)\mathrm{sk}(e^{\hat{\xi}\theta})^{\vee}$ for $|\theta| < \pi, \mathrm{sk}(e^{\hat{\xi}\theta}) := (1/2)(e^{\hat{\xi}\theta} - e^{-\hat{\xi}\theta}) \in so(3)$ [26]. Then, since $\theta/\sin\theta > 0$ holds for $|\theta| < \pi$, the same calculation technique as in the proof of Lemma 9.2 in [19] yields

$$\begin{aligned}\dot{\phi}(e^{\hat{\xi}\theta_{w\beta}}) \leq k_e \textstyle\sum_{j\in\mathcal{N}_\beta} \frac{\theta_{w\beta}}{\sin\theta_{w\beta}} \frac{\theta_{\beta j}}{\sin\theta_{\beta j}} (\cos\theta_{w\beta} \\ - \cos\theta_{wj} - \cos\theta_{w\beta}(1 - \cos\theta_{\beta j})).\end{aligned}$$

Finally, since $1 - \cos\theta_{\beta j} \geq 0$, $\cos\theta_{w\beta} > 0$ (from $|\theta_{w\beta}| < \pi/2$), and $|\theta_{w\beta}| \geq |\theta_{wj}|$ (i.e., $\cos\theta_{w\beta} \leq \cos\theta_{wj}$) hold for $j \in \mathcal{N}_\beta$ from the definition of rigid body β, we obtain $\dot{\phi}(e^{\hat{\xi}\theta_{w\beta}}) \leq 0$, which completes the proof. ■

ACKNOWLEDGMENT

The authors would like to thank Mr. A. Kodama and Mr. Y. Tadokoro for their valuable technical support.

REFERENCES

[1] E. Shaw, "Fish in schools," *Natur. Hist.*, vol. 84, no. 8, pp. 40–46, 1975.
[2] A. Okubo, "Dynamical aspects of animal grouping: Swarms, schools, flocks and herds," *Adv. Biophys.*, vol. 22, pp. 1–94, 1986.
[3] C. W. Reynolds, "Flocks, herds and schools: A distributed behavioral model," *Comput. Graph.*, vol. 21, no. 4, pp. 25–34, Jul. 1987.
[4] J. Toner and Y. Tu, "Flocks, herds, and schools: A quantitative theory of flocking," *Phys. Rev. E*, vol. 58, no. 4, pp. 4828–4858, Oct. 1998.
[5] A. Czirók, M. Vicsek, and T. Vicsek, "Collective motion of organisms in three dimensions," *Physica A*, vol. 264, no. 1–2, pp. 299–304, Feb. 1999.
[6] I. D. Couzin, J. Krause, R. James, G. D. Ruxton, and N. R. Franks, "Collective memory and spatial sorting in animal groups," *J. Theor. Biol.*, vol. 218, no. 1, pp. 1–11, Sep. 2002.
[7] M. Ballerini *et al.*, "Interaction ruling animal collective behavior depends on topological rather than metric distance: Evidence from a field study," *Proc. Natl. Acad. Sci. USA*, vol. 105, no. 4, pp. 1232–1237, Jan. 2008.
[8] N. Maruyama, D. Saito, Y. Hashimoto, and T. Ikegami, "Dynamic organization of flocking behaviors in a large-scale boids model," *J. Comput. Soc. Sci.*, vol. 2, pp. 77–84, Mar. 2019.
[9] G. Vásárhelyi *et al.*, "Optimized flocking of autonomous drones in confined environments," *Sci. Robot.*, vol. 3, no. 20, Jul. 2018, Art. no. eaat3536.
[10] R. Olfati-Saber, "Flocking for multi-agent dynamic systems: Algorithms and theory," *IEEE Trans. Autom. Control*, vol. 51, no. 3, pp. 401–420, Mar. 2006.
[11] K. Saulnier, D. Saldaña, A. Prorok, G. J. Pappas, and V. Kumar, "Resilient flocking for mobile robot teams," *IEEE Robot. Autom. Lett.*, vol. 2, no. 2, pp. 1039–1046, Apr. 2017.
[12] G. Vásárhelyi *et al.*, "Outdoor flocking and formation flight with autonomous aerial robots," in *Proc. IEEE/RSJ Int. Conf. Int. Robots Syst.*, 2014, pp. 3866–3873.
[13] W. Li and M. W. Spong, "Analysis of flocking of cooperative multiple inertial agents via a geometric decomposition technique," *IEEE Trans. Syst., Man, Cybern. Syst.*, vol. 44, no. 12, pp. 1611–1623, Dec. 2014.
[14] K. D. Do, "Flocking for multiple elliptical agents with limited communication ranges," *IEEE Trans. Robot.*, vol. 27, no. 5, pp. 931–942, Oct. 2011.
[15] L. A. R. Reyes and H. G. Tanner, "Flocking, formation control, and path following for a group of mobile robots," *IEEE Trans. Control Syst. Technol.*, vol. 23, no. 4, pp. 1268–1282, Jul. 2015.
[16] S. Hauert *et al.*, "Reynolds flocking in reality with fixed-wing robots: Communication range vs. maximum turning rate," in *Proc. IEEE/RSJ Int. Conf. Int. Robots Syst.*, 2011. pp. 5015–5020.
[17] M. Khaledyan, T. Liu, V. Fernandez-Kim, and M. de Querioz, "Flocking and target interception control for formations of nonholonomic kinematic agents," *IEEE Trans. Control Syst. Technol.*, to be published.
[18] N. Moshtagh and A. Jadbabaie, "Distributed geodesic control laws for flocking of nonholonomic agents," *IEEE Trans. Autom. Control*, vol. 52, no. 4, pp. 681–686, Apr. 2007.
[19] T. Hatanaka, N. Chopra, M. Fujita, and M. W. Spong, *Passivity-Based Control and Estimation in Networked Robotics*. Cham, Switzerland: Springer, 2015.
[20] L. Wang, A. D. Ames, and M. Egerstedt, "Safety barrier certificates for collisions-free multirobot systems," *IEEE Trans. Robot.*, vol. 33, no. 3, pp. 661–674, Jun. 2017.
[21] A. D. Ames, X. Xu, J. W. Grizzle, and P. Tabuada, "Control barrier function based quadratic programs for safety critical systems," *IEEE Trans. Autom. Control*, vol. 62, no. 8, pp. 3861–3876, Aug. 2017.
[22] R. M. Murray, Z. Li, and S. S. Sastry, *A Mathematical Introduction to Robotic Manipulation*. Boca Raton, FL, USA: CRC Press, 1994.
[23] M. Mesbahi and M. Egerstedt, *Graph Theoretic Methods for Multiagent Networks*. Princeton, NJ, USA: Princeton University Press, 2010.
[24] E. Montijano, E. Cristofalo, D. Zhou, M. Schwager, and C. Sagüés, "Vision-based distributed formation control without an external positioning system," *IEEE Trans. Robot.*, vol. 32, no. 2, pp. 339–351, Apr. 2016.
[25] T. Ibuki, T. Hatanaka, M. Fujita, and M. W. Spong, "Visual feedback pose synchronization with a generalized camera model," in *Proc. 50th IEEE Conf. Decis. Control Eur. Control Conf.*, 2011, pp. 4999–5004.
[26] F. Bullo and R. M. Murray, "Proportional derivative (PD) control on the Euclidean group," in *Proc. Eur. Control Conf.*, 1995, pp. 1091–1097.
[27] H. K. Khalil: *Nonlinear Systems*, 3rd ed. Upper Saddle River, NJ, USA: Prentice Hall, 2002.
[28] S. Boyd and L. Vandenberghe, *Convex Optimization*. Cambridge, UK: Cambridge University Press, 2004.
[29] L. Wang, A. D. Ames, and M. Egerstedt, "Multi-objective compositions for collision-free connectivity maintenance in teams of mobile robots," in *Proc. 55th IEEE Conf. Decis. Control*, 2016, pp. 2659–2664.
[30] D. Pickem *et al.*, "The Robotarium: A remotely accessible swarm robotics research testbed," in *Proc. IEEE Int. Conf. Robot. Autom.*, 2017, pp. 1699–1706.
[31] VICON. Motion Capture Systems. [Online]. Available: https://www.vicon.com/ (Last accessed 2020-02-24).
[32] G. Casalino, M. Aicardi, A. Bicchi, and A. Balestrino, "Closed-loop steering for unicycle-like vehicles: A simple Lyapunov like approach," *IFAC Proc. Vol.*, vol. 27, no. 14, pp. 335–342, Sep. 1994.